ELSEVIER

Journal of Crystal Growth 231 (2001) 371–390

JOURNAL OF CRYSTAL GROWTH

www.elsevier.com/locate/jcrysgro

Modeling of threading dislocation reduction in growing GaN layers

S.K. Mathis[a,1], A.E. Romanov[b], L.F. Chen[a], G.E. Beltz[c], W. Pompe[d], J.S. Speck[a,*]

[a] *Materials Department, University of California, Santa Barbara, CA 93106, USA*
[b] *A.F. Ioffe Physico-Technical Institute, Russian Academy of Sciences, 194021 St. Petersburg, Russia*
[c] *Mechanical Engineering Department, University of California, Santa Barbara, CA 93106, USA*
[d] *Institut für Werkstoffwissenschaft, Technische Universtität Dresden, Hallwachsstr. 3, 01069 Dresden, Germany*

Abstract

In this work, a model is developed to treat threading dislocation (TD) reduction in (0 0 0 1) wurtzite epitaxial GaN thin films. The model is based on an approach originally proposed for (0 0 1) FCC thin film growth and uses the concepts of mutual TD motion and reactions. We show that the experimentally observed slow TD reduction in GaN can be explained by low TD reaction probabilities due to TD line directions practically normal to the film surface. The behavior of screw dislocations in III-nitride films is considered and is found to strongly impact TD reduction. Dislocation reduction data in hydride vapor phase epitaxy (HVPE) grown GaN are well described by this model. The model provides an explanation for the non-saturating TD density in thick GaN films. © 2001 Elsevier Science B.V. All rights reserved.

Keywords: A1. Line defects; A3. Hydride vapor phase epitaxy; A3. Metalorganic chemical vapor deposition; B1. Nitrides

1. Introduction

Gallium nitride based semiconducting materials grown directly on available substrates have high dislocation densities. Extended defects such as dislocations and stacking faults are known to have a reduced effect on device operation in GaN, but at sufficiently high densities, threading dislocations (TDs) adversely affect device properties. For example, at TD densities above about $5\times10^{9}\,\mathrm{cm}^{-2}$, non-radiative recombination at dislocations limits light emitting diode efficiencies [1,2]. TDs also act as charged scattering centers and reduce carrier mobilities [3]. Leakage current in reverse-biased p–n junctions is reduced when TD densities are decreased [4]. In nitride-based semiconductors, TDs themselves are not mobile during device operation [5], but they have been shown to act as a fast diffusion pathway for Mg dopants [6]. Thus, threading dislocations densities in the range of 1×10^{8}–$1\times10^{10}\,\mathrm{cm}^{-2}$ in GaN may

*Corresponding author. Tel.: +1-805-893-8005; fax: +1-805-893-8983.
E-mail address: speck@mrl.ucsb.edu (J.S. Speck).
[1] Current address: Agilent Technologies, 350 West Trimble Road, MS 90UB, San Jose, CA 95131-1008, USA.

0022-0248/01/$ - see front matter © 2001 Elsevier Science B.V. All rights reserved.
PII: S 0 0 2 2 - 0 2 4 8 (0 1) 0 1 4 6 8 - 3

ultimately limit device applications, even with a short minority carrier diffusion length on the order of 50 nm.

The conventional method of reducing TD density in semiconductor films uses either graded or constant composition buffer layers. This method has had success in reducing TD densities in cubic semiconductor systems such as SiGe/Si or InGaAs/GaAs [7,8]. In growing (0 0 1) zincblende semiconductor films, dislocations lie on inclined (1 1 1) slip planes. As growth proceeds, they can meet each other and react, lowering the TD density. It was demonstrated that TD density in constant composition FCC semiconductor buffer layers depends on layer thickness (h) as $1/h$ [9]. The situation is different in the nitride semiconductors, which have the hexagonal wurtzite structure. Experimentally, the line directions of the majority of TDs were observed to be normal to the film/substrate interface and parallel to the [0 0 0 1] direction [10]. Detailed analyses demonstrate that the majority of these TDs are edge (Burgers vector $\mathbf{b} = \langle 1\,1\,\bar{2}\,0 \rangle$) dislocations and some screw ($\mathbf{b} = \langle 0\,0\,0\,1 \rangle$) dislocations [11]. We will show that the mixed dislocations ($\mathbf{b} = \frac{1}{3}\langle 1\,1\,\bar{2}\,3 \rangle$) are inclined at approximately 12° to the film normal. For this reason (and we will demonstrate this in our calculations), buffer layers have had limited success in reducing TD densities in GaN. In a recent study using hydride vapor phase epitaxy (HVPE), a dislocation density of low to mid-$10^6\,\mathrm{cm}^{-2}$ was observed after 300 μm of growth [12]. This represents a large reduction in TD density compared with the $\sim 10^9$–$10^{10}\,\mathrm{cm}^{-2}$ typically observed in 1–5 μm thick films.

GaN has a high mismatch with the substrates on which it is generally grown, sapphire and SiC. In the case of GaN on sapphire, the lattice parameter mismatch is ~14.6% [11]. GaN films on sapphire are grown in MOCVD using a standard two-step process. Prior to the first growth step, the sapphire substrate is heated to high temperature (HT, 1000–1100°C) and cleaned with flowing hydrogen (~5–30 min). Then, while maintaining high temperature, the sapphire substrate may then be exposed to ammonia (prenitridation). The substrate temperature is then reduced to typically 500–600°C (LT) and a nucleation layer is grown with a nominal thickness of ~200 Å. The nucleation layer (NL) structure is composed of three dimensional facetted, predominantly cubic (1 1 1) oriented GaN grains. Adjacent NL grains only contact one another at their base, which has been attributed to the high energy necessary to coalesce islands with a large degree of stacking disorder. After the NL growth, the film is heated to the normal growth temperature of 1050°C and the cubic GaN NL partially transforms to hexagonal GaN. Larger (~1 μm) size islands ('HT islands') nucleate on the LT layer. Isolated HT islands laterally overgrow the nucleation layer without generating any threading dislocations. Rather, all disorder between the NL islands and individual HT islands is accommodated by Shockley and Frank partial dislocations with line directions in the (0 0 0 1) plane, or by local strain. The threading dislocations are generated as a result of coalescence of adjacent HT islands. Rotation about the [0 0 0 1] direction leads to pure tilt boundaries and rotation about directions [*uvt*0] results in vertical twist boundaries. Thus, the majority of threading dislocations in GaN, grown under optimized conditions, result from coalescence of HT islands. Typical TD densities are in the range mid-10^8–mid-$10^9\,\mathrm{cm}^{-2}$ using this method. It is possible to extensively prenitride the sapphire at HT. This generally results in a highly columnar microstructure consisting of only pure edge TDs arranged in tilt boundaries with a density in the low $10^{10}\,\mathrm{cm}^{-2}$-range.

The aim of the present work is to understand the TD reduction mechanism in GaN films and to explain the weaker TD density reduction in comparison with cubic semiconductor buffer layers. This is done by adapting a prior model for TD density falloff in FCC thin films to the case of [0 0 0 1] oriented hexagonal semiconductors [9,13]. First, experimental observations of TD types (screw, edge, and mixed dislocations) and densities are considered. The possible dislocation reactions, such as fusion or annihilation, are determined for each of the 20 possible threading dislocations in GaN. Relative probabilities are determined for each of these reactions based on crystallographic considerations. Coupled differential equations are used to model the TD density evolution with changing film thickness. Using experimental observations, the model's validity is evaluated. Finally, implications of the model for screw dislocation behavior are considered. The connection between growth initiation conditions and TD density falloff in GaN is discussed.

2. Background

2.1. Types of TDs in GaN

Fig. 1(a) shows the unit cell of GaN, which has the wurtzite structure. The commonly observed Burgers vectors for unit dislocations in the wurtzite structure include the $\pm\mathbf{c}$ and $\pm\mathbf{a}_i$ ($i = 1-3$) lattice translation vectors and their sums $\pm\mathbf{c}\pm\mathbf{a}_i$. The **c** translation is 62% larger than the **a** translation, making dislocations with Burgers vectors $\mathbf{b} = \mathbf{c}$ or $\mathbf{b} = \mathbf{c} + \mathbf{a}$ which have higher energies than $\mathbf{b} = \mathbf{a}$ dislocations. These dislocations in the wurtzite lattice and their reactions have been previously investigated [14].

As described above, the majority of TDs in GaN result from coalescence of misoriented islands. Edge TDs ($\mathbf{b} = \mathbf{a}_\mathrm{I} = \frac{1}{3}\langle 2\,\bar{1}\,\bar{1}\,0\rangle$) result from coalescence of islands with a misorientation about the [0 0 0 1] axis. Arrays of parallel edge TDs form low angle tilt boundaries. The geometry of edge dislocations in GaN is shown in Fig. 1(b). The line direction of these dislocations is [0 0 0 1] and the Burgers vectors are one of the three basal plane crystal axes and their inverses, which include $\pm\mathbf{a}_1 = \frac{1}{3}[2\,\bar{1}\,\bar{1}\,0]$, $\pm\mathbf{a}_2 = \frac{1}{3}[\bar{1}\,2\,\bar{1}\,0]$, and $\pm\mathbf{a}_3 = \frac{1}{3}[\bar{1}\,\bar{1}\,2\,0]$, and are perpendicular to the dislocation line. Burgers vector analysis in transmission electron microscopy has revealed that edge dislocations make up a significant fraction of the total TD

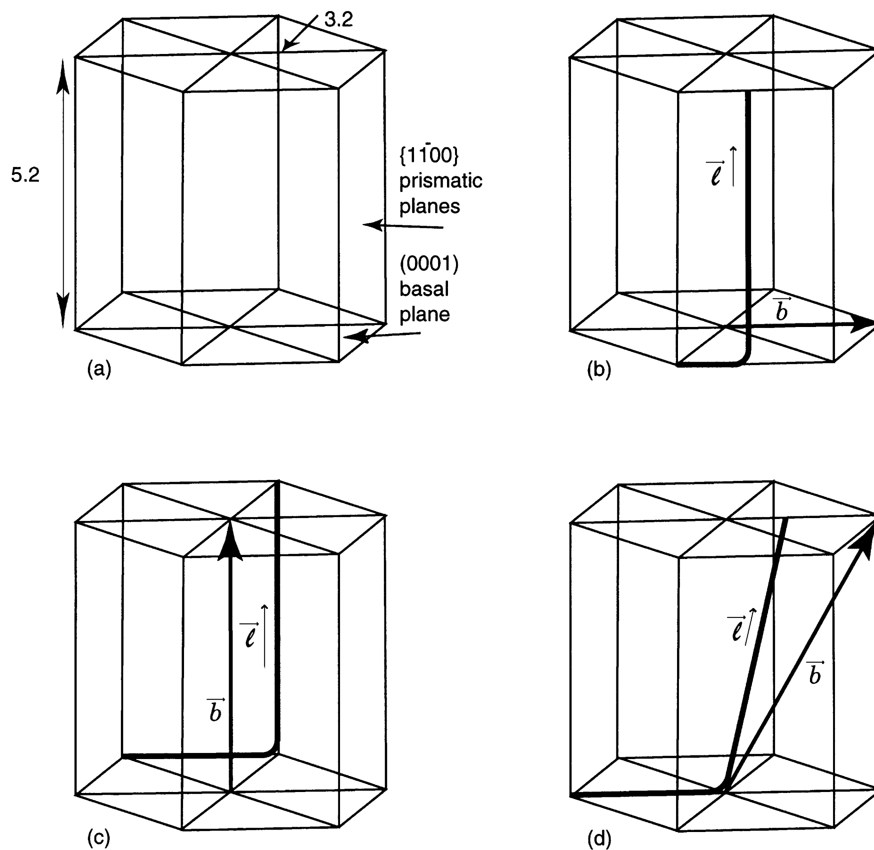

Fig. 1. GaN crystallography. (a) The GaN unit cell has $c = 1.62a$. (b) Edge dislocations in GaN with Burgers vectors of the type $\frac{1}{3}\langle 1\,1\,\bar{2}\,0\rangle$ and a vertical line direction. (c) Perfect screw dislocations with $\mathbf{b} = \pm[0\,0\,0\,1]$ and line direction [0 0 0 1]. (d) Mixed character dislocations with Burgers vectors of the type $\frac{1}{3}\langle 1\,1\,\bar{2}\,3\rangle$ and inclined line directions.

density in high-quality MOCVD films [11,15]. Additionally, it appears that the edge character dislocations represent a larger fraction of the total TD density in thicker films. Wu et al. examined both 1 and 5 μm thick films grown under identical conditions and showed that the edge TDs make up 40% of the total TD density in 1 μm thick MOCVD-grown films, while after 5 μm of growth, they make up 70% of all TDs [11].

Pure screw dislocations are the most uncommon type of TD in GaN films. Both their line direction and Burgers vector lie along the [0 0 0 1] direction, as shown schematically in Fig. 1(c). Published TEM measurements usually put screw dislocations at <1 to 10% of the overall TD density in MOCVD-grown material [16]. Wu et al. reported that pure screw TDs had a very small proportion (much less than 1%) of the total TD density in MOCVD-grown GaN [11]. However, it has been reported that in MBE-initiated GaN growth on sapphire, screw dislocations have been found to represent 20% of the overall TD density [15]. Nanopipes, which are sometimes observed in GaN films grown on SiC and on sapphire, have been associated with open-core screw dislocations [17]. Nanopipes are surrounded by growth spirals at the film surface, indicating a **c**-component Burgers vector dislocation at their centers [17]. However, nanopipes appear not to have appreciable density in high-quality material, and often screw dislocations have closed cores [16]. It is not presently understood why open core dislocations occur, or why screw dislocations have low density in epitaxial GaN films [18].

Burgers vectors for mixed dislocations are $\mathbf{b} = \mathbf{c} + \mathbf{a}_i = \frac{1}{3}\langle 1\,1\,\bar{2}\,3\rangle$. The reported fraction of mixed dislocations varies from 2% of the total density in the case of MBE-initiated growth to 68% in metalorganic vapor phase epitaxy-grown (MOVPE-grown) material [15,16]. As mixed dislocations are the only TDs with an (energetically favored) inclined line direction relative to the film normal (this point will be developed below), they are the only TDs moving laterally relative to other TDs during growth. The geometry of a mixed dislocation is shown in Fig. 1(d). As we will show, they drive TD reduction by reacting with other dislocations. The microstructure of a 1.4 μm-thick MBE-grown film on a 1.6 μm-thick MOCVD layer of GaN on sapphire is shown in Fig. 2. Growth conditions for this sample are described in Ref. [19]. This cross-section TEM picture was imaged in the $\mathbf{g} = 0\,0\,0\,2$ diffraction condition, under which only dislocations with screw character are visible. Since the proportion of pure screw ($\mathbf{b} = \mathbf{c}$) dislocations is very low, essentially all of the dislocations imaged are mixed-character ($\mathbf{b} = \mathbf{a} + \mathbf{c}$) dislocations. We assume that the maximum angle between the surface normal and the dislocation line direction will be the true angle of

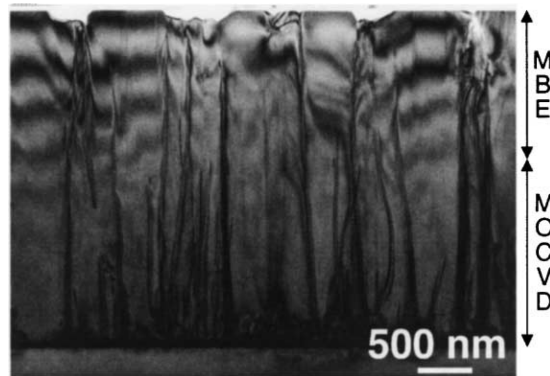

Fig. 2. Cross-section TEM micrograph of 1.4 μm MBE-grown GaN on a 1.6 μm MOCVD-grown GaN buffer. Micrograph taken under $\mathbf{g} = 0\,0\,0\,2$ imaging condition. Under this imaging condition, only dislocations with a **c**-component Burgers vector are visible. Due to the low screw TD density, the dislocations are predominantly of mixed screw-edge character with line direction inclined at $\sim 12.2^\circ$ to the surface normal. This angle was determined by taking the maximum inclination angle at sufficient distance from the film/substrate interface so that TD generation conditions did not dictate line direction. The maximum inclination was used because TDs lying in the plane normal to the viewing direction would have the largest apparent inclination, while those aligned with the viewing direction or at an angle $<90^\circ$ would have a smaller apparent inclination.

deviation, as only one slip plane is positioned normal to the viewing direction. This angle was measured to be approximately 12.2°.

2.2. Modeling of TD reduction in FCC semiconductors

Romanov et al. have developed a model for dislocation density evolution in growing films for (0 0 1) oriented FCC materials (see Refs. [9,13]). We adapt the model to the case of GaN hexagonal materials in this paper, so the essential features of this model are described here. There are 24 unique combinations of dislocation slip plane and Burgers vector in FCC semiconductors. These consist of four possible {1 1 1} type slip planes and 6 Burgers vectors (including sign inversions) per slip plane of the type $1/2\langle 1\,1\,0\rangle$. Threading dislocations may result from either island coalescence or stress-driven nucleation processes. For the latter case, dislocations are believed to be generated by surface-initiated processes leading to half-loops, with a misfit dislocation and two associated threading segments [20]. Most misfit dislocations in FCC semiconductors are the so-called 60° dislocations, with Burgers vectors that are inclined at 60° to the dislocation line direction.

Fusion or annihilation reactions are the primary mechanisms for TD density reduction in thin films. Dislocations may react with one another when they are in close proximity. A fusion reaction occurs when two TD lines become one TD with the new Burgers vector $\mathbf{b}_3 = \mathbf{b}_1 + \mathbf{b}_2$. An annihilation reaction happens when two TD lines with opposite Burgers vectors ($\mathbf{b}_1 = -\mathbf{b}_2$) undergo the reaction $\mathbf{b}_1 + \mathbf{b}_2 = 0$, removing the dislocations entirely. The similar reactions specific to GaN films will be considered in detail in the following sections.

Dislocations may meet and react with increasing film thickness. TDs do not experience misfit stress-induced motion in a relaxed layer, but rather their relative motion is due to their inclined line directions. As the film thickness increases, the point of intersection of inclined TDs with the surface moves laterally. When one TD interacts with another TD in FCC semiconductors, it has a 1 in 24 chance of an annihilation reaction and a 6 in 24 chance for a fusion reaction. For each TD family, a differential equation was written that represents the density evolution with thickness. The resulting 24 coupled differential equations were then solved numerically.

The overall TD density ρ can also be described by a simplified equation [21]

$$d\rho = -K\rho^2\,dh, \tag{1}$$

where K is considered to be a dislocation reaction cross-section (kinetic reaction coefficient). K is proportional to the dislocation annihilation radius r_A, but also is a function of the analogous dislocation fusion reaction radius r_F when fusion reactions are included. In these calculations, K is assumed to be independent of thickness. The initial condition for this equation is a known TD density $\rho(h = h_0) = \rho_0$ at some thickness h_0. The solution of Eq. (1) is given as

$$\rho = \frac{1/K}{h + \hat{h}}, \tag{2}$$

where the parameter $\hat{h}$ corresponds to the initial threading dislocation density and is defined by the relation

$$\hat{h} = (K\rho_0)^{-1} - h_0. \tag{3}$$

For TDs to react, they must come within a reaction distance r_I of one another, where $r_I = r_A$ or r_F. The reaction distance r_I is governed by the type of material (the Peierls barrier) and the temperature. This distance (annihilation or fusion radius) has been previously estimated to be between 500 and 5000 Å in FCC semiconductors [9]. Recently, calculations have confirmed this range of annihilation radii [22]. From experimental data, r_A has been evaluated to be $\sim$1000 Å in GaAs films at the ordinary growth temperature (580°C) [23].

The results of this TD reduction model reproduce the experimentally observed $\sim 1/h$ dependency of TD density on thickness at large h. Compared with GaN, TDs in FCC semiconductors are always reduced more quickly with increasing film thickness due to their inclined line directions.

3. Dislocation reduction model for GaN

3.1. Dislocation reactions

There are 20 unique types of dislocations in GaN—each defined by their Burgers vector and line direction. For example, there are two different types of screw dislocations, with Burgers vector $\mathbf{b} = \pm[0\,0\,0\,1]$. Additionally, six different edge dislocations and 12 different mixed character dislocations exist in the nitrides. The driving force for TD reactions is the minimization of film free energy. The line energy of the dislocation is proportional to b^2, so the criterion for successful TD reactions is

$$b_1^2 + b_2^2 \geqslant b_3^2. \tag{4}$$

This is the 'b^2-criterion' [21]. The reaction is still driven to completion if the left and right hand terms of Eq. (4) are equal since this removes one dislocation line, thereby reducing the overall energy (removal of one TD core). Each of the 20 possible TD types is listed in Table 1 with its reactions and TDs produced through the reaction, if any. Several of these reactions produce compound Burgers vector dislocations. For example, the following reaction is energetically favored

$$(\mathbf{a}_3 - \mathbf{c}) + (-\mathbf{a}_2 + \mathbf{c}) \to (\mathbf{a}_3 - \mathbf{a}_2) \tag{5}$$

since the b^2 criterion is satisfied. However, the reaction will continue with another step:

$$(\mathbf{a}_3 - \mathbf{a}_2) \to (\mathbf{a}_3) + (-\mathbf{a}_2) \tag{6}$$

to form two separate dislocations, numbers 4 and 5 in Table 1. The reaction in Eq. (6) is energetically favorable according to the b^2-criterion. The resulting dislocations will be driven apart from one another because there is an angle of 60° between $\mathbf{a}_3$ and $-\mathbf{a}_2$. There are several such compound reactions in this system, which are driven primarily by the large reduction in strain energy due to the removal of the $\mathbf{c}$ component of the Burgers vector in mixed dislocations. We note that 'two-to-two' compound reactions are not predicted for FCC (0 0 1) epitaxy.

3.2. TD line directions

The TD line direction can be determined by minimizing the dislocation energy, which results from a competition between minimizing the dislocation line length and maximizing the screw character of the TD. We follow here the calculations of line direction performed for the case of a dislocation in (0 0 1) oriented FCC semiconductors as described in Ref. [9]. The core energy is assumed to be independent of the dislocation type in the first approximation for this calculation, but as we will discuss, the screw and edge dislocation core energies may be different. In the isotropic approximation, the elastic strain energy in the lattice surrounding the dislocation is greater for an edge dislocation than for a screw dislocation with the same length Burgers vector. The dislocation type is determined by the angle ϕ between the Burgers vector $\mathbf{b}$ and the dislocation line $\mathbf{l}$. A dislocation is pure edge for $\phi = 90^\circ$ and pure screw for $\phi = 0^\circ$. The angles relevant to the calculation of line direction are shown in Fig. 3. The strain energy depends on ϕ and h:

$$E(h, \phi) = \frac{\mu \mathbf{b}^2}{4\pi} \frac{h}{\cos(\theta - \phi)} \left(\cos^2\phi + \frac{\sin^2\phi}{1 - v} \right) \ln\left(\frac{\alpha R}{|\mathbf{b}|} \right). \tag{7}$$

Table 1

Reaction table for threading dislocations (TDs) in growing GaN layers. The reactions that are not possible either due to the b^2 criterion or for geometric reasons are indicated with a "—" while reactions that are possible are indicated with their designated number. Reactions that produce two dislocations are denoted with two numbers corresponding to their products

		1	2	3	4	5	6	7	8	9	10	11	12	13	14	15	16	17	18	19	20
		a_1	$-a_1$	a_2	$-a_2$	a_3	$-a_3$	a_1+c	a_1-c	$-a_1+c$	$-a_1-c$	a_2+c	a_2-c	$-a_2+c$	$-a_2-c$	a_3+c	a_3-c	$-a_3+c$	$-a_3-c$	c	$-c$
1	a_1	—	—	—	—	—	—	—	—	19	20	17	18	—	—	13	14	—	—	—	—
2	$-a_1$	—	—	—	—	—	—	19	20	—	—	—	—	15	16	—	—	11	12	—	—
3	a_2	—	—	—	—	—	—	17	18	—	—	—	—	19	20	9	10	—	—	—	—
4	$-a_2$	—	—	—	—	—	—	—	—	15	16	19	20	—	—	—	—	7	8	—	—
5	a_3	—	—	—	—	—	—	13	14	—	—	9	10	—	—	—	—	19	20	—	—
6	$-a_3$	—	—	—	—	—	—	—	—	11	12	—	—	7	8	19	20	—	—	—	—
7	a_1+c	—	19	17	—	13	—	—	1&1	—	A	—	6	—	1&4	—	4	—	1&6	—	1
8	a_1-c	—	20	18	—	14	—	1&1	—	A	—	6	—	1&4	—	4	—	1&6	—	1	—
9	$-a_1+c$	19	—	—	15	—	11	—	A	—	2&2	—	2&3	—	5	—	2&5	—	3	—	2
10	$-a_1-c$	20	—	—	16	—	12	A	—	2&2	—	2&3	—	5	—	2&5	—	3	—	2	—
11	a_2+c	17	—	—	19	9	—	—	6	—	2&3	—	3&3	—	A	—	2	—	3&6	—	3
12	a_2-c	18	—	—	20	10	—	6	—	2&3	—	3&3	—	A	—	2	—	3&6	—	3	—
13	$-a_2+c$	—	15	19	—	—	7	—	1&4	—	5	—	A	—	4&4	—	4&5	—	1	—	4
14	$-a_2-c$	—	16	20	—	—	8	1&4	—	5	—	A	—	4&4	—	4&5	—	1	—	4	—
15	a_3+c	13	—	9	—	—	19	—	4	—	2&5	—	2	—	4&5	—	5&5	—	A	—	5
16	a_3-c	14	—	10	—	—	20	4	—	2&5	—	2	—	4&5	—	5&5	—	A	—	5	—
17	$-a_3+c$	—	11	—	7	19	—	—	1&6	—	3	—	3&6	—	1	—	A	—	6&6	—	6
18	$-a_3-c$	—	12	—	8	20	—	1&6	—	3	—	3&6	—	1	—	A	—	6&6	—	6	—
19	c	—	—	—	—	—	—	—	1	—	2	—	3	—	4	—	5	—	6	—	—
20	$-c$	—	—	—	—	—	—	1	—	2	—	3	—	4	—	5	—	6	—	—	—

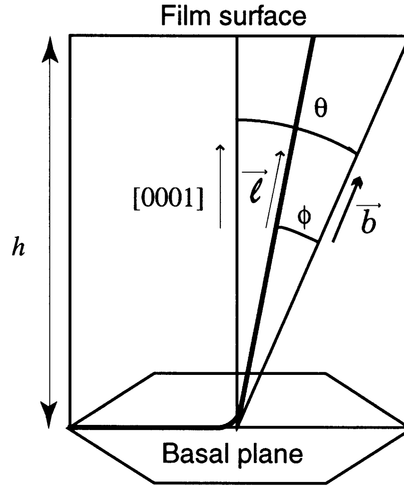

Fig. 3. Angles used in calculation of line direction. ϕ is the angle between the Burgers vector and line direction. θ is the angle between the Burgers vector and [0 0 0 1], which is the shortest possible line direction for GaN dislocations in (0 0 0 1) film growth.

Here, μ is the shear modulus, v is Poisson's ratio, R is the screening length for the dislocation energy calculation, and α is chosen to take into account the contribution of the dislocation core. θ is the angle between **b** and [0 0 0 1], which is the direction of the shortest possible line length for TDs in (0 0 0 1) GaN films. For simplicity we use the isotropic approximation for elastic constants. In calculating the line direction for a TD at a given thickness, the Burgers vector and film thickness are fixed, so **b**, h and θ are constant. The energy is then minimized by setting $\partial E/\partial \phi = 0$ and solving for ϕ. For $\mathbf{b} = \pm \mathbf{a}_i$ TDs, $\phi = 90^\circ$ and for $\mathbf{b} = \pm \mathbf{c}$ dislocations, $\phi = 0^\circ$. That is, the line direction is [0 0 0 1] for both edge and screw TDs, reconfirming experimental observations. For the mixed $\mathbf{b} = \pm(\mathbf{a}_i \pm \mathbf{c})$ dislocations, the line direction is inclined to the film normal at $\theta - \phi = 15.6^\circ$. This agrees well with the experimental observation of inclined line directions at $\theta - \phi \approx 12^\circ$. Other authors have shown that these line directions may not be accurate for TDs in close proximity to the film/substrate interface [24,25]. However, this work is concerned with the case of dislocation reduction far from the thickness at which TDs are generated.

3.3. Model equations

From the reaction table, a series of 20 differential equations can be written. They are of the form

$$\frac{\mathrm{d}\rho_i}{\mathrm{d}h} = -\sum_j K_{ij}\rho_i\rho_j + \sum_l \sum_m K_{lm}\rho_l\rho_m. \tag{8}$$

Here, the ρ_i represent the density of a specific TD family, with number designations given in Table 1. The first summation is for the annihilation and fusion reactions, which reduce the density of the ith family TDs by one per reaction. The second summation is for fusion reactions between other families l and m that produce dislocations in the ith family. The K_{ij} are the kinetic coefficients that describe the rate of reactions between dislocations from families i and j.

$$K_{ij} = 2r_\mathrm{I}\left|\frac{\sqrt{1-(\mathbf{l}_i\cdot\mathbf{n}_f)^2)}}{\mathbf{l}_i\cdot\mathbf{n}_f}\frac{[\mathbf{l}_i-(\mathbf{l}_i\cdot\mathbf{n}_f)\mathbf{n}_f]}{|\mathbf{l}_i-(\mathbf{l}_i\cdot\mathbf{n}_f)\mathbf{n}_f|} - \frac{\sqrt{1-(\mathbf{l}_j\cdot\mathbf{n}_f)^2}}{\mathbf{l}_j\cdot\mathbf{n}_f}\frac{[\mathbf{l}_j-(\mathbf{l}_j\cdot\mathbf{n}_f)\mathbf{n}_f]}{|\mathbf{l}_j-(\mathbf{l}_j\cdot\mathbf{n}_f)\mathbf{n}_f|}\right|, \tag{9}$$

where the $\mathbf{l}_i$ are the ith family dislocation line directions and $\mathbf{n}_f$ is the film normal [9]. In the following numerical calculations, we use dimensionless variables by replacing the K_{ij} with $\tilde{K}_{ij} = K_{ij}/2r_\mathrm{I}$ and the ρ_i with $\tilde{\rho}_i = \rho_{ij} r_\mathrm{I}^2$. For simplicity, we took r_A to be constant for all reactions and $r_\mathrm{F} = r_\mathrm{A}$ in this model. In this calculation, the reaction probability depends solely on the line direction of the dislocations and not on the slip planes of the TDs. In fact, this is a simplification as each dislocation has a distinct line direction/Burgers vector combination and therefore a different Peierls barrier to dislocation motion. It has also been assumed that the TDs may move out of their slip planes due to elevated growth temperatures and proximity to the surface of the sample, which is a source and sink for point defects. This non-conservative motion allows only the distance between the TDs, and not the slip planes on which they lie, to dictate the reaction rate for any pair of TDs. The full system of coupled differential equations is included in Appendix A. The calculated coefficients $\tilde{K}_{ij} = K_{ij}/2r_\mathrm{I}$ are included in Appendix B.

4. Results of numerical solutions

4.1. Allowed dislocation reactions and initial conditions

There have been few direct observations of screw dislocation behavior in GaN, so we assume three conditions for GaN screw TDs in the model. (1) In the first case, screw dislocations are assumed to behave in the same way as edge and mixed dislocations; they react with other dislocations and are produced by reactions between other dislocation pairs. (2) The second case assumes that screw dislocations are not capable of reacting with other dislocations. This might happen, for example, if the screw dislocation exists at the center of a growth hillock or at the center of a nanopipe. In the case of a growth hillock, mixed dislocations must elongate and move across the hillock to reach the screw dislocation, making reaction less likely. Open core dislocation motion requires mass transport. Thus, reactions involving screw dislocations could be less likely. Additionally, dislocation reactions that produce screw dislocations might also be less likely if their core energy is large, since the production of a screw dislocation would be energetically costly. The core structure of screw dislocations is different from that of mixed or edge-type dislocations since the core bonds are not broken, but highly stretched. (3) The third condition investigated was an elevated reactivity for screw dislocations. This would lead to a lower screw dislocation density since the screw dislocations would have a larger annihilation radius (for example due to cross-slip) and would be rapidly reduced through reaction.

The six initial conditions used in these calculations are summarized in Table 2. Cases 1 and 3 have 70% edge dislocations and 30% mixed dislocations. These proportions were reported for MOCVD-grown material [26]. Cases 2, 4 and 6 had density distributions given as 60% edge, 30% mixed, and 10% screw. These cases were taken for comparison between low- and high-screw TD density material. Finally, Case 5 was initially given a much higher proportion of mixed character TDs, with 30% edge and 70% mixed dislocations. This was done to compare high mixed TD content and high edge TD content films. In the modeling, the total initial density was set at $1 \times 10^{10}\,\mathrm{cm}^{-2}$ for all cases and the initial density distribution is summarized in Table 2. Neither the Peierls stress nor the annihilation radius has been estimated for GaN, thus we assume an annihilation radius of 500 Å for ordinary growth conditions. We assume that the annihilation radius in GaN will be smaller than that in GaAs due to the generally higher Peierls stresses in hexagonal materials. Later, we will show that this value is consistent with the experimental data. Within the model, this corresponds to a dimensionless initial TD density of $\tilde{\rho}_i^\circ = 0.25$. The initial density of each family of dislocations (unique Burgers vector) was calculated by first dividing the density between the three types of TDs (screw, edge, and mixed), and then dividing the density evenly between the families within that dislocation type. For example, Case 1 would have 30% of the total TD density as mixed dislocations, and

Table 2
Threading dislocation cases used in calculations. Cases 1–6 are summarized, with initial edge, mixed, and screw subdensities and screw dislocation behavior

	Subdensity (%)			Screw dislocation behavior
	Edge	Mixed	Screw	(Generation is screw formation at coalescence, reactions refer to screw as reactants or products)
1	70	30	0	$\rho_s^0 = \rho_s(h) = 0$ Screw generation and reaction prohibited
2	60	30	10	$\rho_s^0 = \rho_s(h) \neq 0$ Screw generation allowed, reaction prohibited
3	70	30	0	$\rho_s^0 = 0 \neq \rho_s(h)$ Screw generation prohibited, reaction allowed
4	60	30	10	$\rho_s^0 \neq 0 \neq \rho_s(h)$ Screw generation and reaction allowed
5A	30	70	0	$\rho_s^0 = \rho_s(h) = 0$ Screw generation and reaction prohibited, high mixed TD density and low edge TD density
5B	98	2	0	$\rho_s^0 = \rho_s(h) = 0$ Screw generation and reaction prohibited, high mixed TD density and low edge TD density
6	60	30	10	$\rho_s^0 \neq 0 \neq \rho_s(h)$ $10\times$ higher annihilation radius for screw TDs

that density would then be evenly divided among the twelve mixed TD families. The 20 coupled differential equations were then solved numerically. For Cases 3, 4, and 6, the calculation included all reactions that were determined to be energetically possible from the b^2-criterion. Case 6 was given an increased probability of screw TD reaction by increasing the reaction radius by one order of magnitude for reactions involving screw TDs. Cases 1, 2 and 5 excluded the possibility of screw dislocations reacting with other dislocations or being formed by reactions between edge and mixed dislocations (the reaction cross-sections K_{ij} were zero for reactions involving screw dislocations for Cases 1, 2 and 5).

4.2. Solutions for TD densities

4.2.1. Overall comparison of Cases 1 to 6

Fig. 4(a) shows the dislocation density evolution with thickness for Cases 1, 2, 3 and 4. In each of the following figures, the normalized TD density ($\tilde{\rho}_{TD} = \rho_{TD} \cdot r_A^2$) is plotted against the normalized thickness ($\tilde{h} = h/r_A$). The TD density for Cases 3 and 4 reduces initially with increasing thickness, but reaches a saturation value. The TD density for Cases 1 and 2, by contrast, continues to reduce with increasing thickness. Case 1, which has no initial screw TD density and no screw TDs formed by reaction with thickness, has the lowest final TD density after a thickness of $h/r_A = 1000\,\mu m/500\,\text{Å} = 20\,000$ (normalized thickness). In Fig. 4(b), a curve fit to the results of Case 1 shows that the data are well described by the relation

$$\rho_{TD} = \frac{1}{Kh^{2/3} + \hat{h}}. \quad (10)$$

From the curve fit, the normalized values for K and $\hat{h}$ are 0.057 and 3.70, respectively. The origin of this dependence on $h^{-2/3}$ is not understood at present and is a topic of ongoing investigation.

Lower initial screw TD density leads to a lower final TD density. For example, Case 1 has an initial screw TD density of zero, and when compared to Case 2 (which had the same reaction conditions), the final TD

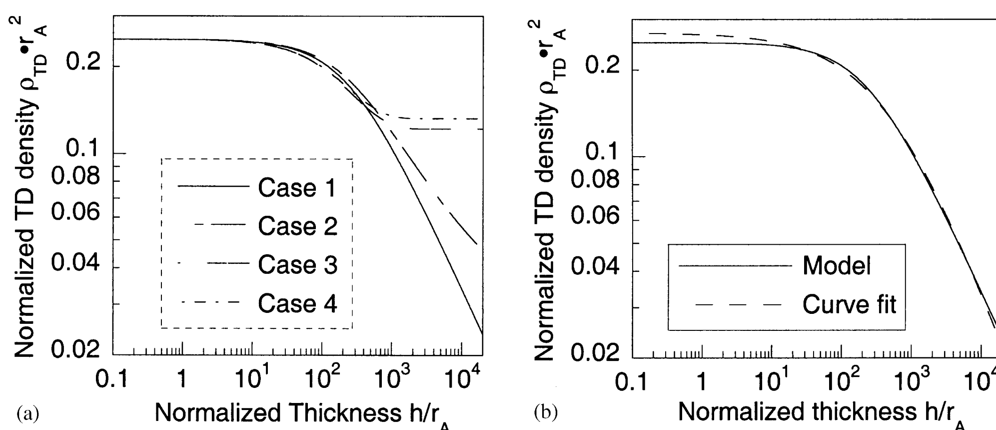

Fig. 4. Total TD density evolution with film thickness for Cases 1–4. (a) Cases 1 and 2, with no screw dislocation reactions allowed, do not display saturation behavior. Cases 3 and 4, with screw dislocation reactions allowed, reach a minimum TD density and saturate. Case 2, with an initial screw TD subdensity of 10% of the total TD density, has a higher final TD density than that of Case 1, which had no screw TDs. Similarly, Case 4, with an initial non-zero screw subdensity, saturated at a higher TD density than Case 3. Maximum thickness corresponds to 250 μm for an annihilation radius of $r_A = 500$Å. (b) A curve fit of Case 1 shows that TD density depends on $1/h^{2/3}$ for large h. The best fit was found with $\rho_{TD} r_A^2 = 1/[0.057(h/r_A)^{2/3} + 3.70]$.

density is lower for Case 1. This is to be expected, as in both Cases 1 and 2, no screw TD reactions are allowed, and therefore, the screw TDs are not removed in Case 2. Cases 3 and 4, which did have screw TD reactions included, show a similar trend: an initial screw TD density leaves a higher final TD density for Case 4.

High, low, and normal screw dislocation annihilation radius cases are shown in Fig. 5. When screw TDs are not allowed to react, as in Case 2, the lowest final TD density is reached since there is no saturation of the total TD density. Case 4, which has screw TDs with the calculated reactivity K_{ij} (normal annihilation radius), initially reduces TD density more slowly than Case 6, which has screw dislocations with $10 \times r_A$ and therefore $10 \times K_{ij}$. However, the TD density for Case 6 saturates sooner with thickness and at a higher TD density than Case 4. The reason is that faster reactions between screw and mixed TDs result in fewer mixed TDs available for reaction with edge TDs. Therefore, all TDs are vertical after the mixed TD content is depleted and no further reactions are possible.

The subdensity evolution of edge, mixed, and screw-type dislocations are shown in Fig. 6. Case 2, with no screw dislocation reactions, is shown in Fig. 6(a). The screw TD density remains constant with thickness, while the edge and mixed TD content falls without saturation. For Case 4, shown in Fig. 6(b), the initial TD subdensities are the same as for Case 2. However, the TD reactions involving screw dislocations are allowed in this case. The result is that mixed TD content falls more quickly with thickness than for Case 2. This is due to both the screw-mixed reactions producing vertical edge dislocations, and the edge-mixed reactions producing vertical screw dislocations. As a result, the mixed TD density becomes so low as to prevent further interaction among TDs, with the end result a saturation in TD density. Fig. 6(c) shows the subdensities for Case 6, where the screw TDs are more reactive than Cases 1–5. Although both screw and edge TD densities decrease, the mixed dislocations are depleted quickly with thickness as in Case 4, and the TD density saturates.

Cases 5A and 5B are shown together in Fig. 7. In both cases, screw TD reactions were not allowed. Case 5A, with high mixed TD density (70% mixed and 30% edge TDs), attains a lower TD density overall than Case 5B. Case 5B has 98% edge TDs and 2% mixed TDs. The TD density does not saturate in either Case

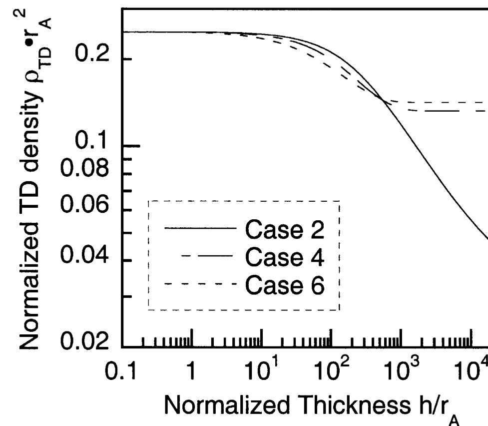

Fig. 5. TD density falls off for Cases 2, 4 and 6. Case 2, with 60% edge, 30% mixed, and 10% screw dislocations, but no allowed screw dislocation reactions, results in no TD density saturation. Cases 4 and 6, with the same initial TD subdensities, had screw reactions allowed. Case 4, with normal screw TD reactivity (r_A and K_{ij}), saturated at a lower TD density than Case 6, which had a high screw reactivity (r_A and K_{ij} were an order of magnitude larger).

5A or Case 5B. The plot shows that a high mixed TD density can reduce the overall TD density further than for high initial edge TD density.

To recap, the results show that screw dislocations impede dislocation reduction when they are allowed to react. Increasing the screw dislocation annihilation radius makes overall dislocation density reduction even less effective. Additionally, a high initial proportion of edge TDs leads to slower TD reduction than a high proportion of mixed TDs.

4.2.2. Effect of annihilation radius

The annihilation radius r_A is an effective reaction rate constant for TD density evolution with increasing film thickness. The total TD density change was calculated for four different values of r_A. The initial TD density of $10^{10}\,\text{cm}^{-2}$ was divided into 40% edge, 50% mixed, and 10% screw character dislocations, where the screw TDs were allowed to react normally as in Case 4. These proportions were reported experimentally for hydride vapor phase epitaxial growth on sapphire [24]. The TD density (in units of cm^{-2}) for $r_A = (300, 500, 1000, \text{and } 2000\,\text{Å})$ is shown in Fig. 8. While the initial rate of TD reduction $\mathrm{d}\rho/\mathrm{d}h$ is faster for higher annihilation radii, the final value of TD density at saturation is the same for each case.

There are few reports in the literature for TD density variation with thickness in thin films of nitride semiconductors. One recent study by Golan et al. on HVPE grown material reported TD density measurements at large thicknesses by plan view TEM [12]. Golan et al. also included high resolution X-ray diffraction measurements for both on-axis and off-axis reflections at successive thicknesses up to 300 μm. We are able to convert these measurements to TD densities using the general proportionality between the peak width of X-ray rocking curves (full width at half maximum, or FWHM) and TD density ($\rho_\perp$) (originally developed by Gay et al. [27] for polycrystalline metals and adapted to the case of thin single crystalline films by Ayers [28]):

$$\rho_\perp^{1/2} \propto \text{FWHM}. \tag{11}$$

A constant of proportionality was found at each of the thicknesses, where TD density and rocking curve widths were measured. This constant was then averaged and the resulting TD density data are shown in Fig. 9. We therefore evaluate our model in terms of agreement with the observed TD density falloff from

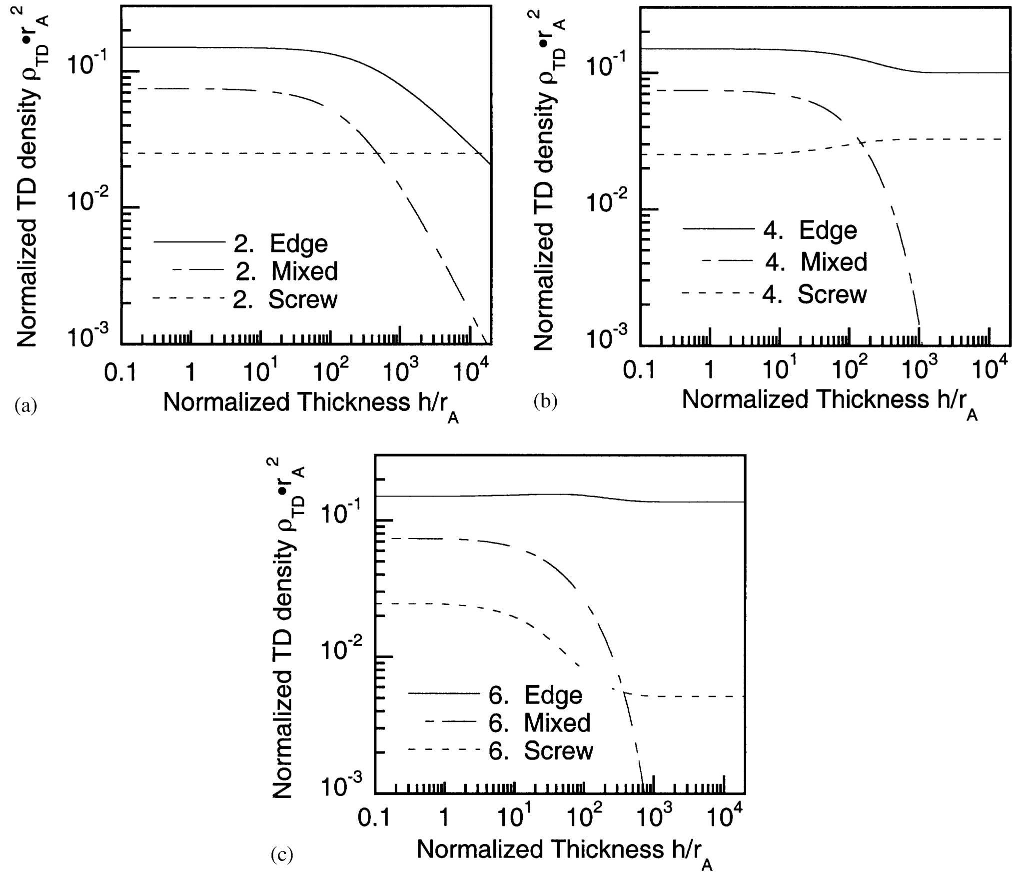

Fig. 6. Subdensity comparison for Cases 2, 4 and 6, each having 60% edge, 30% mixed, and 10% screw dislocation densities initially. (a) Case 2. Screw dislocations, which were not allowed to react, have a constant density. Edge and mixed TD densities fall without saturating. (b) Case 4. Screw TDs are allowed to react, and their density increases, then saturates with thickness. The edge dislocation density also saturates. This saturation happens at a thickness corresponding to the point when the mixed TD density falls suddenly, or when the mixed TDs are depleted. (c) Case 6. Screw TDs are $10\times$ as reactive as in Case 4. The screw and edge TD density both decrease with thickness, but saturate when mixed TDs are depleted. This happens at a smaller thickness and a larger TD density.

this study. The data have been fitted to Eq. (2) with good agreement, as shown. A value of 275 Å for K gives the best fit. Recalling that $K \sim r_A$, we find that TDs in GaN are relatively less reactive than in GaAs under the conventional growth conditions for each material. Lower reactivity means that a higher applied force is required to move TDs in GaN, so a closer approach is required for TD reactions to take place. Therefore, our assumption of 500 Å for the annihilation radius was reasonable for these calculations. We note that the annihilation radius depends strongly on the growth temperature and may also depend on the growth technique [23]. Additionally, there is no observed saturation of TD density at large film thickness in these experimental data. Finally, for comparison with the model, the experimental data were fitted according to the equation

$$\rho_{TD} = \frac{1}{Kh^n + \hat{h}}, \tag{12}$$

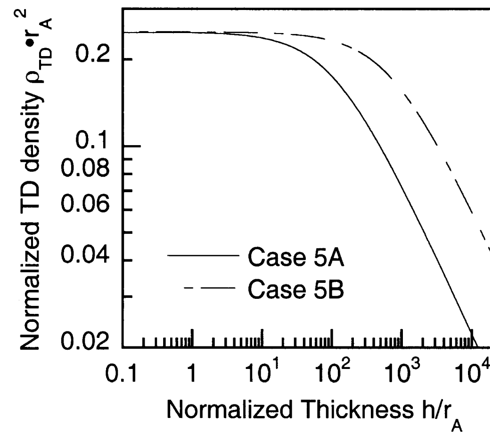

Fig. 7. Density comparison for Cases 1 and 5, with no screw TD reactions allowed. Case 1, with 70% edge, 30% mixed, and no screw dislocations, declines without reaching saturation, but Case 5 attains a lower TD density for all thicknesses. Case 5, with 30% edge, 70% mixed, and no screw TDs, shows that a high proportion of mixed character TDs drives TD density reduction more effectively.

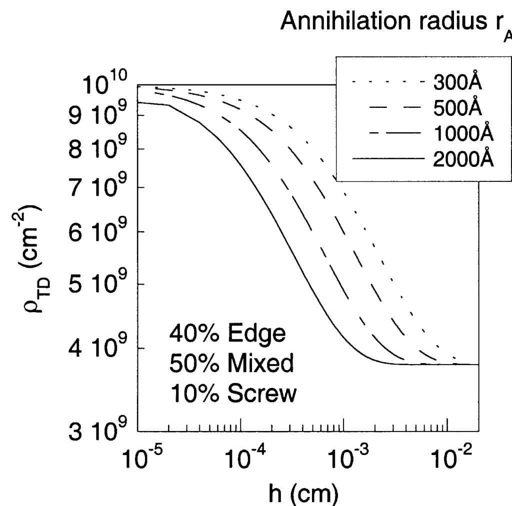

Fig. 8. The effect of annihilation radius on total TD density. Total TD density evolution for r_A values of 300, 500, 2000 and 5000 Å. Screw dislocations reactions were allowed, resulting in the saturation of the total TD density. Saturation occurs at higher thicknesses for lower annihilation radii due to slower reactions between TDs, but the TD density at saturation is the same for the constant initial TD density of 10^{10}/cm^2 and equal initial subdensities.

where K, n, and $\hat{h}$ were allowed to vary. An exponent of $n = 0.66$ is found and it is in good agreement with the model curve fit shown in Fig. 4(b).

5. Discussion

The implication of the presented model is that films with higher initial mixed TD content lead to more extensive TD reduction than films with high edge TD content, all other parameters being equal. These

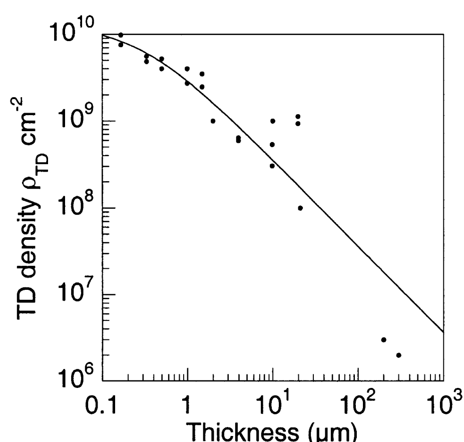

Fig. 9. Experimental GaN dislocation density data. The data from Ref. [11] were fitted with Eq. (2), giving a value for $K \sim 275$ Å and $K \sim r_A$. When the experimental data are not weighted, an exponent $n = 0.66$ is found (for $\rho_{TD} \propto 1/h^n$).

mixed Burgers vector TDs drive the reactions in all cases due to their inclined line direction. This is supported by experimental observations of diminishing mixed character TD fraction and increasing edge TD fraction with film thickness by Wu et al. [11].

The model is suggestive about possible peculiar behavior for screw TDs in GaN. The experimental TD reduction conditions are best reproduced by the model when the screw TDs are not allowed to form or react. The other model for screw dislocation behavior, namely higher r_A and K_{ij} for screw TDs, failed to reproduce experimental observations. An increased annihilation radius for screw TDs might possibly arise if screw TDs were able to glide and undergo cross slip between $\{1\,\bar{1}\,0\,0\}$ slip planes, as suggested previously by Kapolnek et al. [26]. By increasing the screw dislocation reactivity, however, the mixed TDs were depleted more quickly, leading to TD density saturation at smaller thicknesses than when screw TDs were given the calculated K_{ij} from Eq. (9).

Currently, we do not have an explanation for the absence or very low density of pure screw character TDs in epitaxial GaN films. The screw TDs may have anomalously high core energies which prohibit their formation. Alternatively, the screw TDs may form open cores which reduce their mobility and reactivity.

It is possible to control the proportion of edge, mixed, and screw TDs in GaN films to a certain extent. Keller et al. termed the two major types of microstructure in GaN films type A and type B [29]. Type A material, which is grown on a sapphire substrate subjected to a short prenitridation step, was shown to have a relatively high mixed Burgers vector TD content by Heying et al. [30]. Type B material, with a columnar microstructure, had tilt boundaries consisting almost exclusively of edge dislocations, also confirmed by Heying et al. [30]. Cases 5A and 5B give a qualitative comparison between high mixed and high edge dislocation content films. Case 5A, which had 30% edge, 70% mixed, and no screw dislocations, experiences fast TD reduction when compared to Case 5B. Case 5B, with 98% edge, 2% mixed, and no screw dislocations, shows that a higher proportion of edge TDs is detrimental for TD reduction. In summary, the microstructure of type A material should (and does) result in lower TD density due to the initially higher mixed TD content.

Surface treatment conditions should be chosen in all of the GaN growth techniques to produce optimal TD distributions. In MOCVD growth, these conditions have been found and chosen to minimize columnar, edge TD-dominated growth. However, the HVPE material considered in this paper had no surface pretreatment [12]. It has been speculated that surface pretreatment in MOCVD leads to sapphire surface

roughening, which then produces the optimal low-temperature-grown nucleation layer [12]. The initiation conditions must be chosen to have a balance of pure edge and mixed character TDs.

Buffer layers in (0 0 0 1) wurtzite thin films are not as useful in dislocation density reduction as buffers on (0 0 1) zincblende semiconductors. Typical mismatched buffer layer thicknesses to achieve high-quality device growth in zincblende semiconductors are on the order of 1–10 μm. In the case of GaAs or InGaAs buffers, typical growth temperatures are in the range of 500–580°C and growth rates are on the order of 1 μm/h. In the work of Golan et al., a GaN buffer layer thickness of 300 μm was required to achieve a threading dislocation density of $2 \times 10^6\,\mathrm{cm}^{-2}$ [12]. In addition to the much higher mismatch and different growth physics, the growth temperature of GaN is typically more than 1000°C. Clearly, the application of a standard buffer layer to threading dislocation reduction in GaN is not realistic for any growth technique except hydride vapor phase epitaxy, where ~ 100 μm/h growth rates are achieved. In terms of our model, the inclined line direction of all dislocation types in zincblende films, along with the larger reaction radii for cubic semiconductors (1200 Å for GaAs compared with 275 Å for GaN), mean that dislocation reduction is efficient in cubic thin films.

6. Conclusions

In conclusion, we have applied a model for TD evolution initially proposed for (0 0 1) oriented FCC thin film growth to (0 0 0 1) GaN growth. We have shown that TD reduction in GaN is driven primarily by reactions between edge and mixed character TDs. Our model has demonstrated the following:

- The line direction of each of the three types of TDs in GaN (edge, screw, and mixed) was calculated using energetic considerations and confirmed with experimental data. The TD line directions were found to be [0 0 0 1] for edge and screw TDs and inclined at 15.6° with respect to [0 0 0 1] for mixed TDs.
- The experimental TD reduction observations are best modeled when screw dislocations are not involved in TD reactions. This may be due to a lower screw TD mobility, which in turn may be due to high screw dislocation core energy. This idea is supported by prior experimental observations of low screw dislocation subdensities and open core screw dislocations with smaller than expected Burgers vectors.
- The model shows that films with a high fraction of edge TDs do not have significant TD density reduction. Mixed character TDs drive reduction reactions because they are the only dislocations with inclined line directions. Inclined TD line directions make mutual lateral TD motion possible with increasing film thickness.

Finally, our model shows that hydride vapor phase epitaxy is a viable method for TD reduction in GaN if mixed character TD subdensity is maximized and films are grown extremely thick.

Acknowledgements

The authors would like to thank Y. Golan, B. Heying, M.C. Hansen, and H. Marchand for useful discussions. JSS and SKM are grateful for support from NSF Travel Grant award number INT-9603242. This work was supported by the AFOSR PRET Center (Dr. Gerald Witt, contract monitor). AER was supported in part by Grant 97-3006 from the Russian Research Council "Physics of Solid Nanostructures" and by DFG project 422.

Appendix A. Full differential equations

In the appendix, the differential equations are listed in non-normalized form. In the calculation, the normalized form with $\tilde{\rho}_i$ and $\tilde{K}_{ij}$ were used. Here, the density of each TD subfamily is given as ρ_i and the first derivative with respect to h is denoted as $\mathrm{d}\rho_i/\mathrm{d}h$.

$$\begin{aligned}\mathrm{d}\rho_1/\mathrm{d}h = & -\rho_1(K_{1,9}\rho_9 + K_{1,10}\rho_{10} + K_{1,11}\rho_{11} + K_{1,12}\rho_{12} + K_{1,15}\rho_{15} + K_{1,16}\rho_{16}) \\ & + 2K_{7,8}\rho_7\rho_8 + K_{7,14}\rho_7\rho_{14} + K_{7,18}\rho_7\rho_{18} + K_{7,20}\rho_7\rho_{20} + K_{8,13}\rho_8\rho_{13} + K_{8,17}\rho_8\rho_{17} + K_{8,19}\rho_8\rho_{19} \\ & + K_{13,18}\rho_{13}\rho_{18} + K_{14,17}\rho_{14}\rho_{17},\end{aligned}$$

$$\begin{aligned}\mathrm{d}\rho_2/\mathrm{d}h = & -\rho_2(K_{2,7}\rho_7 + K_{2,8}\rho_8 + K_{2,13}\rho_{13} + K_{2,14}\rho_{14} + K_{2,17}\rho_{17} + K_{2,18}\rho_{18}) \\ & + 2K_{9,10}\rho_9\rho_{10} + K_{9,12}\rho_9\rho_{12} + K_{9,16}\rho_9\rho_{16} + K_{9,20}\rho_9\rho_{20} + K_{10,11}\rho_{10}\rho_{11} + K_{10,15}\rho_{10}\rho_{15} \\ & + K_{10,19}\rho_{10}\rho_{19} + K_{11,16}\rho_{11}\rho_{16} + K_{12,15}\rho_{12}\rho_{15},\end{aligned}$$

$$\begin{aligned}\mathrm{d}\rho_3/\mathrm{d}h = & -\rho_3(K_{3,7}\rho_7 + K_{3,8}\rho_8 + K_{3,13}\rho_{13} + K_{3,14}\rho_{14} + K_{3,15}\rho_{15} + K_{3,16}\rho_{16}) \\ & + K_{9,12}\rho_9\rho_{12} + K_{9,18}\rho_9\rho_{18} + K_{10,11}\rho_{10}\rho_{11} + K_{10,17}\rho_{10}\rho_{17} + 2K_{11,12}\rho_{11}\rho_{12} + K_{11,18}\rho_{11}\rho_{18} \\ & + K_{11,20}\rho_{11}\rho_{20} + K_{12,17}\rho_{12}\rho_{17} + K_{12,19}\rho_{12}\rho_{19},\end{aligned}$$

$$\begin{aligned}\mathrm{d}\rho_4/\mathrm{d}h = & -\rho_4(K_{4,9}\rho_9 + K_{4,10}\rho_{10} + K_{4,11}\rho_{11} + K_{4,12}\rho_{12} + K_{4,17}\rho_{17} + K_{4,18}\rho_{18}) \\ & + K_{7,14}\rho_7\rho_{14} + K_{7,16}\rho_7\rho_{16} + K_{8,13}\rho_8\rho_{13} + K_{8,15}\rho_8\rho_{15} + 2K_{13,14}\rho_{13}\rho_{14} + K_{13,16}\rho_{13}\rho_{16} \\ & + K_{13,20}\rho_{13}\rho_{20} + K_{14,15}\rho_{14}\rho_{15} + K_{14,19}\rho_{14}\rho_{19},\end{aligned}$$

$$\begin{aligned}\mathrm{d}\rho_5/\mathrm{d}h = & -\rho_5(K_{5,7}\rho_7 + K_{5,8}\rho_8 + K_{5,11}\rho_{11} + K_{5,12}\rho_{12} + K_{5,17}\rho_{17} + K_{5,18}\rho_{18}) \\ & + K_{9,14}\rho_9\rho_{14} + K_{9,16}\rho_9\rho_{16} + K_{10,13}\rho_{10}\rho_{13} + K_{10,15}\rho_{10}\rho_{15} + K_{13,16}\rho_{13}\rho_{16} + K_{14,15}\rho_{14}\rho_{15} \\ & + 2K_{15,16}\rho_{15}\rho_{16} + K_{15,20}\rho_{15}\rho_{20} + K_{16,19}\rho_{16}\rho_{19},\end{aligned}$$

$$\begin{aligned}\mathrm{d}\rho_6/\mathrm{d}h = & -\rho_6(K_{6,9}\rho_9 + K_{6,10}\rho_{10} + K_{6,13}\rho_{13} + K_{6,14}\rho_{14} + K_{6,15}\rho_{15} + K_{6,16}\rho_{16}) \\ & + K_{7,12}\rho_7\rho_{12} + K_{7,18}\rho_7\rho_{18} + K_{8,11}\rho_8\rho_{11} + K_{8,17}\rho_8\rho_{17} + K_{11,18}\rho_{11}\rho_{18} + K_{12,17}\rho_{12}\rho_{17} \\ & + 2K_{17,18}\rho_{17}\rho_{18} + K_{17,20}\rho_{17}\rho_{20} + K_{18,19}\rho_{18}\rho_{19},\end{aligned}$$

$$\begin{aligned}\mathrm{d}\rho_7/\mathrm{d}h = & -K_{7,10}\rho_7\rho_{10} \\ & -\rho_7(K_{2,7}\rho_2 + K_{3,7}\rho_3 + K_{5,7}\rho_5 + K_{7,8}\rho_8 + K_{7,12}\rho_{12} + K_{7,14}\rho_{14} + K_{7,16}\rho_{16} + K_{7,18}\rho_{18} \\ & + K_{7,20}\rho_{20}) + K_{4,17}\rho_4\rho_{17} + K_{6,13}\rho_6\rho_{13},\end{aligned}$$

$$\begin{aligned}\mathrm{d}\rho_8/\mathrm{d}h = & -K_{8,9}\rho_8\rho_9 \\ & -\rho_8(K_{2,8}\rho_2 + K_{3,8}\rho_3 + K_{5,8}\rho_5 + K_{7,8}\rho_7 + K_{8,11}\rho_{11} + K_{8,13}\rho_{13} + K_{8,15}\rho_{15} + K_{8,17}\rho_{17} \\ & + K_{8,19}\rho_{19}) + K_{4,18}\rho_4\rho_{18} + K_{6,14}\rho_6\rho_{14},\end{aligned}$$

$$\begin{aligned}\mathrm{d}\rho_9/\mathrm{d}h = & -K_{8,9}\rho_8\rho_9 \\ & -\rho_9(K_{1,9}\rho_1 + K_{4,9}\rho_4 + K_{6,9}\rho_6 + K_{9,10}\rho_{10} + K_{9,12}\rho_{12} + K_{9,14}\rho_{14} + K_{9,16}\rho_{16} + K_{9,18}\rho_{18} \\ & + K_{9,20}\rho_{20}) + K_{3,15}\rho_3\rho_{15} + K_{5,11}\rho_5\rho_{11},\end{aligned}$$

$$\begin{aligned}\mathrm{d}\rho_{10}/\mathrm{d}h = & -K_{7,10}\rho_7\rho_{10} \\ & -\rho_{10}(K_{1,10}\rho_1 + K_{4,10}\rho_4 + K_{6,10}\rho_6 + K_{9,10}\rho_9 + K_{10,11}\rho_{11} + K_{10,13}\rho_{13} + K_{10,15}\rho_{15} + K_{10,17}\rho_{17} \\ & + K_{10,19}\rho_{19}) + K_{3,16}\rho_3\rho_{16} + K_{5,12}\rho_5\rho_{12},\end{aligned}$$

$$
\begin{aligned}
d\rho_{11}/dh = & -K_{11,14}\rho_{11}\rho_{14} \\
& -\rho_{11}(K_{1,11}\rho_1 + K_{4,11}\rho_4 + K_{5,11}\rho_5 + K_{8,11}\rho_8 + K_{10,11}\rho_{10} + K_{11,12}\rho_{12} + K_{11,16}\rho_{16} + K_{11,18}\rho_{18} \\
& + K_{11,20}\rho_{20}) + K_{2,17}\rho_2\rho_{17} + K_{6,9}\rho_6\rho_9,
\end{aligned}
$$

$$
\begin{aligned}
d\rho_{12}/dh = & -K_{12,13}\rho_{12}\rho_{13} \\
& -\rho_{12}(K_{1,12}\rho_1 + K_{4,12}\rho_4 + K_{5,12}\rho_5 + K_{7,12}\rho_7 + K_{9,12}\rho_9 + K_{11,12}\rho_{11} + K_{12,15}\rho_{15} + K_{12,17}\rho_{17} \\
& + K_{12,19}\rho_{19}) + K_{2,18}\rho_2\rho_{18} + K_{6,10}\rho_6\rho_{10},
\end{aligned}
$$

$$
\begin{aligned}
d\rho_{13}/dh = & -K_{12,13}\rho_{12}\rho_{13} \\
& -\rho_{13}(K_{2,13}\rho_2 + K_{3,13}\rho_3 + K_{6,13}\rho_6 + K_{8,13}\rho_8 + K_{10,13}\rho_{10} + K_{13,14}\rho_{14} + K_{13,16}\rho_{16} + K_{13,18}\rho_{18} \\
& + K_{13,20}\rho_{20}) + K_{1,15}\rho_1\rho_{15} + K_{5,7}\rho_5\rho_7,
\end{aligned}
$$

$$
\begin{aligned}
d\rho_{14}/dh = & -K_{11,14}\rho_{11}\rho_{14} \\
& -\rho_{14}(K_{2,14}\rho_2 + K_{3,14}\rho_3 + K_{6,14}\rho_6 + K_{7,14}\rho_7 + K_{9,14}\rho_9 + K_{13,14}\rho_{13} + K_{14,15}\rho_{15} + K_{14,17}\rho_{17} \\
& + K_{14,19}\rho_{19}) + K_{1,16}\rho_1\rho_{16} + K_{5,8}\rho_5\rho_8,
\end{aligned}
$$

$$
\begin{aligned}
d\rho_{15}/dh = & -K_{15,18}\rho_{15}\rho_{18} \\
& -\rho_{15}(K_{1,15}\rho_1 + K_{3,15}\rho_3 + K_{6,15}\rho_6 + K_{8,15}\rho_8 + K_{10,15}\rho_{10} + K_{12,15}\rho_{12} + K_{14,15}\rho_{14} + K_{15,16}\rho_{16} \\
& + K_{15,20}\rho_{20}) + K_{4,9}\rho_4\rho_9 + K_{2,13}\rho_2\rho_{13},
\end{aligned}
$$

$$
\begin{aligned}
d\rho_{16}/dh = & -K_{16,17}\rho_{16}\rho_{17} \\
& -\rho_{16}(K_{1,16}\rho_1 + K_{3,16}\rho_3 + K_{6,16}\rho_6 + K_{7,16}\rho_7 + K_{9,16}\rho_9 + K_{11,16}\rho_{11} + K_{13,16}\rho_{13} + K_{15,16}\rho_{15} \\
& + K_{16,19}\rho_{19}) + K_{4,10}\rho_4\rho_{10} + K_{2,14}\rho_2\rho_{14},
\end{aligned}
$$

$$
\begin{aligned}
d\rho_{17}/dh = & -K_{16,17}\rho_{16}\rho_{17} \\
& -\rho_{17}(K_{2,17}\rho_2 + K_{4,17}\rho_4 + K_{5,17}\rho_5 + K_{8,17}\rho_8 + K_{10,17}\rho_{10} + K_{12,17}\rho_{12} + K_{14,17}\rho_{14} + K_{17,18}\rho_{18} \\
& + K_{17,20}\rho_{20}) + K_{1,11}\rho_1\rho_{11} + K_{3,7}\rho_3\rho_7,
\end{aligned}
$$

$$
\begin{aligned}
d\rho_{18}/dh = & -K_{15,18}\rho_{15}\rho_{18} \\
& -\rho_{18}(K_{2,18}\rho_2 + K_{4,18}\rho_4 + K_{5,18}\rho_5 + K_{7,18}\rho_7 + K_{9,18}\rho_9 + K_{11,18}\rho_{11} + K_{13,18}\rho_{13} + K_{17,18}\rho_{17} \\
& + K_{18,19}\rho_{19}) + K_{1,12}\rho_1\rho_{12} + K_{3,8}\rho_3\rho_8,
\end{aligned}
$$

$$
\begin{aligned}
d\rho_{19}/dh = & -\rho_{19}(K_{8,19}\rho_8 + K_{10,19}\rho_{10} + K_{12,19}\rho_{12} + K_{14,19}\rho_{14} + K_{16,19}\rho_{16} + K_{18,19}\rho_{18}) \\
& + K_{1,9}\rho_1\rho_9 + K_{2,7}\rho_2\rho_7 + K_{3,13}\rho_3\rho_{13} + K_{4,11}\rho_4\rho_{11} + K_{5,17}\rho_5\rho_{17} + K_{6,15}\rho_6\rho_{15},
\end{aligned}
$$

$$
\begin{aligned}
d\rho_{20}/dh = & -\rho_{20}(K_{7,20}\rho_7 + K_{9,20}\rho_9 + K_{11,20}\rho_{11} + K_{13,20}\rho_{13} + K_{15,20}\rho_{15} + K_{17,20}\rho_{17}) \\
& + K_{1,10}\rho_1\rho_{10} + K_{2,8}\rho_2\rho_8 + K_{3,14}\rho_3\rho_{14} + K_{4,12}\rho_4\rho_{12} + K_{5,18}\rho_5\rho_{18} + K_{6,16}\rho_6\rho_{16}.
\end{aligned}
$$

Appendix B. Reaction coefficients K_{ij}

The reaction coefficients calculated from Eq. (8) are shown in the dimensionless form of $K_{ij}/2r_{\mathrm{I}}$. Reactions determined to be not possible according to the b^2 criterion or for geometrical reasons are listed

with a zero probability. The reaction radius r_I can be either r_A (annihilation) or r_F (fusion). The ratio r_A/r_F was taken to be one in this model for simplicity.

		1	2	3	4	5	6	7	8	9	10	11	12	13	14	15	16	17	18	19	20
		a_1	$-a_1$	a_2	$-a_2$	a_3	$-a_3$	a_1+c	a_1-c	$-a_1+c$	$-a_1-c$	a_2+c	a_2-c	$-a_2+c$	$-a_2-c$	a_3+c	a_3-c	$-a_3+c$	$-a_3-c$	c	−c
1	a_1	0.00	0.00	0.00	0.00	0.00	0.00	0.09	0.15	0.09	0.15	0.09	0.15	0.09	0.15	0.09	0.15	0.09	0.15	0.00	0.00
2	$-a_1$	0.00	0.00	0.00	0.00	0.00	0.00	0.09	0.15	0.09	0.15	0.09	0.15	0.09	0.15	0.09	0.15	0.09	0.15	0.00	0.00
3	a_2	0.00	0.00	0.00	0.00	0.00	0.00	0.09	0.15	0.09	0.15	0.09	0.15	0.09	0.15	0.09	0.15	0.09	0.15	0.00	0.00
4	$-a_2$	0.00	0.00	0.00	0.00	0.00	0.00	0.09	0.15	0.09	0.15	0.09	0.15	0.09	0.15	0.09	0.15	0.09	0.15	0.00	0.00
5	a_3	0.00	0.00	0.00	0.00	0.00	0.00	0.09	0.15	0.09	0.15	0.09	0.15	0.09	0.15	0.09	0.15	0.09	0.15	0.00	0.00
6	$-a_3$	0.00	0.00	0.00	0.00	0.00	0.00	0.09	0.15	0.09	0.15	0.09	0.15	0.09	0.15	0.09	0.15	0.09	0.15	0.00	0.00
7	a_1+c	0.09	0.09	0.09	0.09	0.09	0.09	0.00	0.06	0.17	0.24	0.15	0.21	0.09	0.13	0.15	0.21	0.09	0.13	0.09	0.09
8	a_1-c	0.15	0.15	0.15	0.15	0.15	.0.15	0.06	0.00	0.24	0.30	0.21	0.26	0.13	0.15	0.21	0.26	0.13	0.15	0.15	0.15
9	$-a+c$	0.09	0.09	0.09	0.09	0.09	0.09	0.17	0.24	0.00	0.06	0.09	0.13	0.15	0.21	0.09	0.13	0.15	0.21	0.09	0.09
10	$-a_1-c$	0.15	0.15	0.15	0.15	0.15	0.15	0.24	0.30	0.06	0.00	0.13	0.15	0.21	0.26	0.13	0.15	0.21	0.26	0.15	0.15
11	a_2+c	0.09	0.09	0.09	0.09	0.09	0.09	0.15	0.21	0.09	0.13	0.00	0.06	0.18	0.24	0.15	0.21	0.09	0.13	0.09	0.09
12	a_2-c	0.15	0.15	0.15	0.15	0.15	0.15	0.21	0.26	0.13	0.15	0.06	0.00	0.24	0.30	0.21	0.26	0.13	0.15	0.15	0.15
13	$-a_2+c$	0.09	0.09	0.09	0.09	0.09	0.09	0.09	0.13	0.15	0.21	0.18	0.24	0.00	0.06	0.09	0.13	0.15	0.21	0.09	0.09
14	$-a_2-c$	0.15	0.15	0.15	0.15	0.15	0.15	0.13	0.15	0.21	0.26	0.24	0.30	0.06	0.00	0.13	0.15	0.21	0.26	0.15	0.15
15	a_3+c	0.09	0.09	0.09	0.09	0.09	0.09	0.15	0.21	0.09	0.13	0.15	0.21	0.09	0.13	0.00	0.06	0.17	0.24	0.09	0.09
16	a_3-c	0.15	0.15	0.15	0.15	0.15	0.15	0.21	0.26	0.13	0.15	0.21	0.26	0.13	0.15	0.06	0.00	0.24	0.30	0.15	0.15
17	$-a_3+c$	0.09	0.09	0.09	0.09	0.09	0.09	0.09	0.13	0.15	0.21	0.09	0.13	0.15	0.21	0.17	0.24	0.00	0.06	0.09	0.09
18	$-a_3-c$	0.15	0.15	0.15	0.15	0.15	0.15	0.13	0.15	0.21	0.26	0.13	0.15	0.21	0.26	0.24	0.30	0.06	0.00	0.15	0.15
19	c	0.00	0.00	0.00	0.00	0.00	0.00	0.09	0.15	0.09	0.15	0.09	0.15	0.09	0.15	0.09	0.15	0.09	0.15	0.00	0.00
20	−c	0.00	0.00	0.00	0.00	0.00	0.00	0.09	0.15	0.09	0.15	0.09	0.15	0.09	0.15	0.09	0.15	0.09	0.15	0.00	0.00

References

[1] S.J. Rosner, E.C. Carr, M.J. Ludowise, G. Girolami, H.I. Erikson, Appl. Phys. Lett. 70 (1997) 420.
[2] T. Sugahara, H. Sato, M. Hao, Y. Naoi, S. Kurai, S. Tottori, K. Yamashita, K. Nishino, L.T. Romano, S. Sakai, Japan. J. Appl. Phys. 37 (1998) L398.
[3] N.G. Weimann, L.F. Eastman, D. Doppalapudi, H.M. Ng, T.D. Moustakas, J. Appl. Phys. 83 (1998) 3656.
[4] P. Kozodoy, J.P. Ibbetson, H. Marchand, P.T. Fini, S. Keller, J.S. Speck, S.P. DenBaars, U.K. Mishra, Appl. Phys. Lett. 73 (1998) 975.
[5] L. Sugiura, J. Appl. Phys. 81 (1997) 1633.
[6] N. Kuroda, C. Sasaoka, A. Kimura, A. Usui, Y. Mochizuki, J. Crystal Growth 189–190 (1998) 551.
[7] M.T. Currie, S.B. Samavedam, T.A. Langdo, C.W. Leitz, E.A. Fitzgerald, Appl. Phys. Lett. 72 (1998) 1718.
[8] M.T. Bulsara, C. Leitz, E.A. Fitzgerald, in: D.L. McDaniel, Jr., M.O. Manasreh, R.H. Miles, S. Sivanathan (Eds.), Infrared Applications of Semiconductors II, Mater. Res. Soc., Warrendale, PA, 1998.
[9] A.E. Romanov, W. Pompe, G. Beltz, J.S. Speck, Phys. Stat. Solidi 198 (1996) 3342.
[10] K.A. Dunn, S.E. Babcock, R. Vaudo, V. Phanse, J. Redwing, in: F.A. Ponce, S.P. DenBaars, B.K. Meyer, S. Nakamura, S. Strite (Eds.), Nitride Semiconductors Symposium, Mater. Res. Soc., Warrendale, PA, 1998, pp. 417–422.
[11] X.-H. Wu, L.M. Brown, D. Kapolnek, S. Keller, B. Keller, S.P. DenBaars, J.S. Speck, J. Appl. Phys. 80 (1996) 3228.
[12] Y. Golan, X.-H. Wu, J.S. Speck, R.P. Vaudo, V.M. Phanse, Appl. Phys. Lett. 73 (1998) 3090.
[13] A.E. Romanov, W. Pompe, G. Beltz, J.S. Speck, Phys. Stat. Solidi 199 (1997) 33.
[14] Y.A. Osipyan, I.S. Smirnova, Phys. Stat. Sol. 30 (1968) 19.
[15] N. Grandjean, J. Massies, P. Vennéguès, M. Leroux, F. Demangeot, M. Renucci, J. Frandon, J. Appl. Phys. 83 (1998) 1379.
[16] Y. Xin, S.J. Pennycook, N.D. Browning, P.D. Nellist, S. Sivananthan, F. Omnès, B. Beaumont, J.P. Faurie, P. Gibart, Appl. Phys. Lett. 72 (1998) 2680.
[17] W. Qian, G.S. Rohrer, M. Skowronski, K. Doverspike, L.B. Rowland, D.K. Gaskill, Appl. Phys. Lett. 67 (1995) 2284.
[18] P. Pirouz, Phil. Mag. A 78 (1998) 727.
[19] B. Heying, R. Averbeck, L.F. Chen, E. Haus, H. Reichert, J.S. Speck, J. Appl. Phys., submitted for publication.

[20] E.A. Fitzgerald, J. Vac. Sci. Technol. B 7 (1989) 782.
[21] J.S. Speck, M.A. Brewer, G. Beltz, A.E. Romanov, W. Pompe, J. Appl. Phys. 80 (1996) 3808.
[22] M. Chang, G. Beltz, S. Mathis, Fall 1998 MRS Proceedings, III–V and IV–V Materials and Processing Challenges for Highly Integrated Microelectronics and Optoelectronics, to be published.
[23] S.K. Mathis, X.H. Wu, A.E. Romanov, J.S. Speck, J. Appl. Phys. 86 (1999) 4836.
[24] L.T. Romano, B.S. Krusor, R.J. Molnar, Appl. Phys. Lett. 71 (1997) 2283.
[25] K.A. Dunn, S.E. Babcock, R. Vaudo, V. Phanse, J. Redwing, in: F.A. Ponce, S.P. DenBaars, B.K. Meyer, S. Nakamura, S. Strite (Eds.), Nitride Semiconductors Symposium, Mater. Res. Soc., Warrendale, PA, 1998, pp. 417–422.
[26] D. Kapolnek, X.H. Wu, B. Heying, S. Keller, B.P. Keller, U.K. Mishra, S.P. DenBaars, J.S. Speck, Appl. Phys. Lett. 67 (1995) 1541.
[27] P. Gay, P.B. Hirsch, A. Kelly, Acta Met. 1 (1953) 315.
[28] J.E. Ayers, J. Crystal Growth 135 (1994) 71.
[29] S. Keller, B.P. Keller, Y.-F. Wu, B. Heying, D. Kapolnek, J.S. Speck, U.K. Mishra, S.P. DenBaars, Appl. Phys. Lett. 68 (1996) 1525.
[30] B. Heying, X.H. Wu, S. Keller, Y. Li, D. Kapolnek, B.P. Keller, S.P. DenBaars, J.S. Speck, Appl. Phys. Lett. 68 (1996) 643.